PCCP

View Online / Journal Homepage
Dynamic Article Links

Cite this: DOI: 10.1039/c2cp41161j

www.rsc.org/pccp

PAPER

Vertical phase separation of conjugated polymer and fullerene bulk heterojunction films induced by high pressure carbon dioxide treatment at ambient temperature†

Ryo Kokubu[ab] **and Yang Yang***[ac]

Received 11th April 2012, Accepted 12th April 2012
DOI: 10.1039/c2cp41161j

The morphology of bulk-heterojunctions (BHJ) is critically important for conjugated polymer and fullerene blend solar cells. To alter the morphology, high pressure (gas phase) carbon dioxide (CO_2) treatment is applied to poly(3-hexyl thiophene) (P3HT) and [6,6]-phenyl-C61 butyric acid methyl ester (PCBM) blend films under ambient temperature. This process can achieve vertically phase separated morphology such that PCBM distributes toward the film surface, which is suggested by secondary ion mass spectroscopy (SIMS), contact angle, X-ray photoelectron spectroscopy (XPS) and cross-sectional scanning electron microscope (SEM) studies. While pristine P3HT films do not show a significant change upon CO_2 treatment, pristine PCBM films are plasticized in high pressure CO_2. Thus, PCBM is selectively plasticized by CO_2 in the blend film and is drawn towards the surface due to depressed surface energy, although P3HT tends to distribute around the surface without CO_2. This stratification process can enhance solar cell performance. 55% improvement is achieved in the power conversion efficiency of the CO_2 treated device compared to the untreated one, indicating that CO_2 treatment can be a good candidate for optimizing the morphology and enhancing the performance of BHJ polymer solar cells.

Introduction

Polymer solar cells have attracted a lot of attention because of their potential as a renewable energy source.[1–3] Their performance was dramatically improved with the advent of the bulk heterojunction (BHJ) structure consisting of an interpenetrating network of a conjugated polymer and a fullerene.[4–6] To enhance the performance of BHJ solar cells, controlling the morphology of the BHJ is critical as is interface investigation.[7,8] Typical approaches to control the morphology of the film made from a blended solution include slow drying of a coated wet film,[9,10] thermal annealing,[11,12] vapor annealing,[13] and using additives.[14,15]

While lateral morphology, such as the grain size and the crystallinity of the donor and acceptor, has been widely focused on, the vertical composition distribution is also an important issue because charges have to be transported vertically to their respective electrodes after they are generated at the donor–acceptor interface of BHJ. Conceptually, electron-donor materials, which allow hole transportation, should gradually distribute towards the anode, and the electron-acceptor materials, which allow electron transportation, should gradually distribute towards the cathode.[8] Otherwise, an unfavorable configuration leads to lower charge collection efficiency and thus lower solar cell performance.

In the most investigated case of poly(3-hexyl thiophene) (P3HT) and [6,6]-phenyl-C61 butyric acid methyl ester (PCBM) blend films, PCBM is desired to distribute toward the surface in a regular, cathode on top, device structure. However, it has been pointed out that P3HT spontaneously tends to distribute towards the surface instead of PCBM because the surface energy of P3HT is smaller than that of PCBM (typically, γ_{P3HT}: 27 mN m^{-2}, γ_{PCBM}: 38 mN m^{-2}).[16] Recently, it was reported that a flipped P3PH:PCBM film shows almost the same photovoltaic performance as an unflipped one.[17] However, even if it is assumed that the contact between the flipped film and anode electrode did not become worse, that work has just suggested that the surface P3HT layers would not block electron transportation to the cathodes. Therefore, the vertical profile and its effect still have to be investigated in detail.

To control the vertical composition distribution in a desired way, some approaches have been investigated in recent years. For instance, blending solvents or additives have been explored to segregate PCBM towards the surface, which utilize differences of solubility and volatility among each solvent.[15,18] Another example

[a] *Department of Materials Science and Engineering, University of California, Los Angeles, 405 Hilgard Avenue, Los Angeles, California 90095, USA. E-mail: yangy@ucla.edu; Fax: +1-310-206-7353; Tel: +1-310-825-4052*
[b] *Furukawa Electric, Co., Ltd., 2-2-3 Marunouchi, Chiyoda-Ku, Tokyo 100-8322, Japan*
[c] *California NanoSystems Institute, University of California, Los Angeles, 570 Westwood Plaza, Los Angeles, California 90095, USA*

† Electronic supplementary information (ESI) available. Each element's SIMS profile, quantitative discussion of XPS, uncropped SEM images and peak information of an emission spectrum. See DOI: 10.1039/c2cp41161j

is that a self-assembled monolayer has been introduced on the substrate (anode buffer layer) surface to segregate P3HT towards the bottom.[19] However, those approaches often sacrifice the solar cell performance because the incorporated species can act as a charge carrier trap and increase the series resistance of the cell. Other fabrication processes, such as quasi bi-layer structure achieved by spin-coating P3HT and PCBM separately from different solvent[20,21] or composition controlled spray coating,[22] have also been investigated to generate an ideal composition distribution avoiding such adverse effects.

It is known that some organic materials including polymers can be plasticized and the morphology can be altered under CO_2 which is usually used in gas, liquid, or super critical phase, and such behavior has been explained by the fact that CO_2 dissolves in an organic material and depresses the glass transition temperature.[23–25] However, it has not been applied to optimize the morphology of a BHJ polymer solar cell so far. It is expected that, with this technique, materials can be plasticized at lower temperatures compared to a thermal annealing process, and the morphology or crystal structure can be controlled by the pressure, temperature, and time.[26,27]

Here we investigate a carbon dioxide (CO_2) treatment process to control the morphology of the film fabricated with the conventional process. We demonstrate that a preferable vertical composition distribution in P3HT:PCBM blend films, PCBM is abundant around the surface, can be generated by gas phase CO_2. We prepared an as cast film which has an amorphous-like morphology without any thermal or solvent annealing. While we realize it is suboptimal, it was referenced as a control device to extract the effect of CO_2 treatment. While some classes of measurement techniques to analyze vertical stratification are widely used,[28] the vertically stratified distributions were analyzed by secondary ion mass spectroscopy (SIMS), contact angle, X-ray photoelectron spectroscopy (XPS), and cross-sectional scanning electron microscopy (SEM). Changes in morphology were observed by using an optical microscope and an atomic force microscope (AFM) after treatment with CO_2. UV-visible light absorption and photoluminescence (PL) spectra of the film were measured to examine the effect of CO_2 treatment on phase separation and molecular packing. We also examined the photovoltaic characteristics of the devices with and without CO_2 treatment. 55% improvement was achieved in efficiency for the treated device compared to the untreated one, indicating that CO_2 treatment can be a good candidate for optimizing the morphology and enhancing the performance of BHJ polymer solar cells.

CO_2 treatments on spin-coated pure P3HT, PCBM and the blend film were carried out by putting the samples into a high pressure vessel into which CO_2 can be introduced as shown in Scheme 1. Treatment pressure was controlled to give a stable gas phase at room temperature (4.7 MPa, approximately 12% lower than the saturation pressure), and the treatment time was varied (see the Experimental section).

Results and discussion

To estimate composition depth distributions in P3HT:PCBM films, sulfur profiles detected by SIMS have been plotted (Fig. 1a), which qualitatively indicate P3HT distributions since P3HT contains sulfur but PCBM doesn't.[28,29] It was confirmed

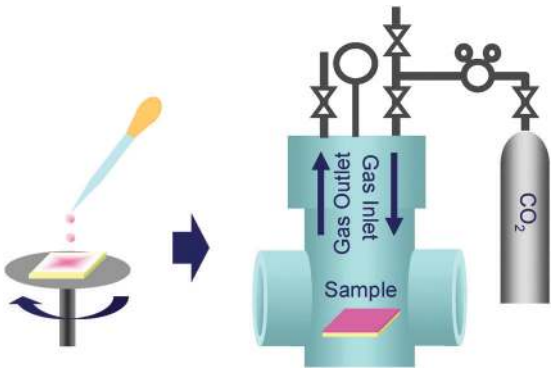

Scheme 1 A schematic illustration of a CO_2 treatment process and an apparatus. Spin-coated samples are put in a high pressure vessel connected with a CO_2 cylinder.

that the PCBM distribution estimated using the oxygen signal is consistent with the one indicated by the sulfur SIMS profile (see ESI† for a comparison of each element's SIMS profile). Before CO_2 treatment (as cast film), P3HT concentration around the surface is higher than in the deeper region, which is in agreement with previous studies attributing this effect to the surface energy difference between P3HT and PCBM.[16] In contrast, P3HT concentration around the surface after 24 hour CO_2 treatment is significantly lower than in the deeper region whose P3HT concentration is increased, which reflects the fact that PCBM concentration is increased around the surface corresponding to the decrease in the deeper region. As the concentration change between the surface and the deeper region is quite precipitous, a PCBM-rich layer is clearly recognizable. Thus, it is clear that PCBM has come out to the surface forming a layer as a result of CO_2 treatment. The 96 hour treated film has a thicker PCBM-rich layer than the 24 hour treated one. While the depth scale of SIMS data has less than $\pm$10% of the error, the PCBM-rich layer thickness is about 32 nm in the 24 hour treated film and about 45 nm in the 96 hour treated one (the interface between the PCBM-rich and P3HT-rich regions has been assumed to be the point at which the sulfur concentration drops to half the value of the flat part of the P3HT-rich region such as the concentration in the range of 100 nm to 150 nm as shown in Fig. 1a).

The contact angle study has supported this trend. The water contact angle of the P3HT:PCBM film surface with CO_2 treatment time has been plotted along with the angles of pristine P3HT and PCBM films in Fig. 1b. The initial contact angle of the P3HT:PCBM film surface is almost the same as the one of pristine P3HT, which supports the SIMS result revealing that P3HT initially distributes towards the surface. The contact angle decreases in proportion to the CO_2 treatment time and reaches the angle of pristine PCBM after the 72 hour CO_2 treatment, which suggests that the surface coverage of PCBM gradually increases and the PCBM-rich layer appears on the surface.

This trend has also been observed by an XPS study which can provide more direct estimations of surface compositions rather than contact angles. The S 2p (S 2p3/2 and S 2p1/2) peaks of the P3HT:PCBM film surface with CO_2 treatment time have been shown in Fig. 1c. (The intensities have been normalized by C 1s peak intensity of each sample.) The sulfur intensity decreases corresponding to CO_2 treatment time and

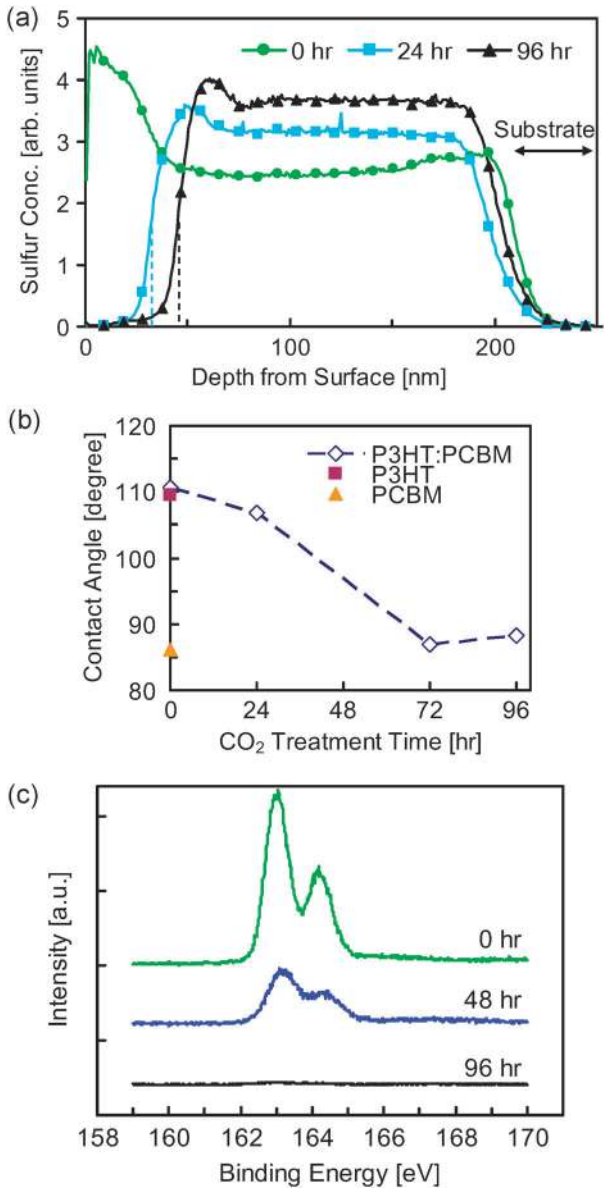

Fig. 1 (a) SIMS profiles of sulfur in P3HT:PCBM blend films before and after CO_2 treatment. Dashed lines indicate the average depth of the interface between the PCBM-rich and the P3HT-rich regions. (b) The water contact angle change of the P3HT:PCBM film surface with CO_2 treatment time. Each data point is the average of ten measurements, and the standard deviation is less than 2°. (c) S 2p region of XPS spectra acquired from the P3HT:PCBM film surface before and after treatment. The intensities have been normalized by their respective C 1s peak intensities.

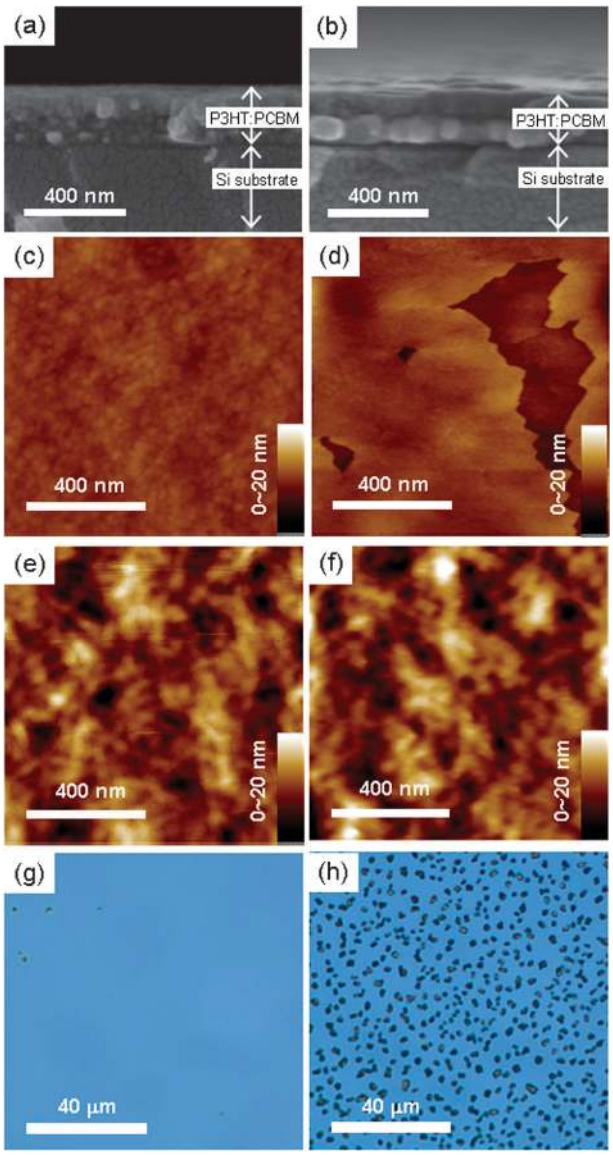

Fig. 2 Cross-sectional SEM images of P3HT:PCBM blend films coated on a silicon substrate; (a) as cast and (b) after 96 hours CO_2 treatment respectively. AFM height images of P3HT:PCBM blend films coated on PEDOT:PSS/ITO/glass substrates; (c) as cast and (d) after 96 hours CO_2 treatment respectively. AFM height images of the pristine P3HT film coated on PEDOT:PSS/ITO/glass substrates; (e) as cast and (f) after 96 hours CO_2 treatment respectively. Optical microscope images of the pristine PCBM film coated on PEDOT:PSS/ITO/glass substrates; (g) as cast and (h) after 96 hours CO_2 treatment respectively.

almost disappears after 96 hour treatment. It is indicated that the P3HT occupancy of the film surface decreases and is significantly altered by PCBM after 96 hour CO_2 treatment. (A brief estimation of quantitative occupancies has been described in ESI.†)

Cross-sectional SEM images of P3HT:PCBM blend films fabricated on a silicon substrate before and after 96 hour CO_2 treatment are shown in Fig. 2a and b respectively (see ESI† for original uncropped images). A contrast between the shallower and the deeper region as well as a layer boundary can be seen clearly in the film after CO_2 treatment, which may support the SIMS result that suggests stratification. In Fig. 2b, the thickness of the top layer which is supposed to be PCBM looks nonuniform and is 40 to 100 nm. This nonuniformity implies that the PCBM layer tends to aggregate on the film surface after further treatment. Since the spot size of the SIMS analysis is 1 mm^2, the thickness estimated from SIMS does not reflect this nonuniformity of the film.

To examine the effect of CO_2 on P3HT and PCBM as well as blend films, each film was fabricated on an indium tin oxide (ITO)/glass substrate covered with poly(3,4-ethylenedioxythiophene):poly(styrene-sulfonic acid) (PEDOT:PSS) and treated with CO_2 for 96 hours and observed by using AFM and optical

microscopy. For the P3HT:PCBM blend film, the AFM images (Fig. 2c and d) have shown a flat plateau structure instead of the lateral morphology after CO_2 treatment, which suggests that the surface is covered with a PCBM-rich layer after CO_2 treatment. In the case of the pristine P3HT film, no significant change was observed after the treatment (Fig. 2e and f respectively). The solubility of gas phase CO_2 in P3HT may not be high enough to plasticize P3HT, to depress the glass transition temperature of P3HT, or to alter its crystal morphology. On the other hand, a dramatic change was observed in pristine PCBM films which aggregated and formed micrometer scale particles (Fig. 2g and h, microscopic images are shown because the scale of the aggregated structure is too large for an AFM observation). It is obvious that PCBM can be plasticized by gas phase CO_2 at room temperature, which leads to the growth of large crystallites.

Those results suggest that CO_2 can selectively plasticize PCBM in P3HT:PCBM blend films and change the structure leading to vertical phase separation. The mechanism of this stratification process at room temperature may be explained by the surface energy difference between P3HT and PCBM. The estimated process is schematically shown in Scheme 2a–f. At first, P3HT tends to be slightly more abundant around the surface in the as cast film because of its lower surface energy (Scheme 2a). Once the film is subjected to high pressure CO_2, the film can impregnate CO_2 which can selectively penetrate through PCBM clusters, and PCBM can be plasticized which reduces its surface energy (Scheme 2b). Also, molecular mobility of PCBM becomes higher, which leads to aggregation and lateral phase separation (Scheme 2c), and simultaneously vertical phase separation can be promoted if the surface energy of plasticized PCBM is lower than that of P3HT (Scheme 2d). Finally, a PCBM-rich layer can be formed on the film surface (Scheme 2e). After CO_2 is released, this stratified structure can be maintained because the molecular mobility of PCBM returns to the original state (Scheme 2f). In this way, CO_2 treatment can generate very unique composition distribution, which cannot be generated by conventional processes such as thermal annealing.

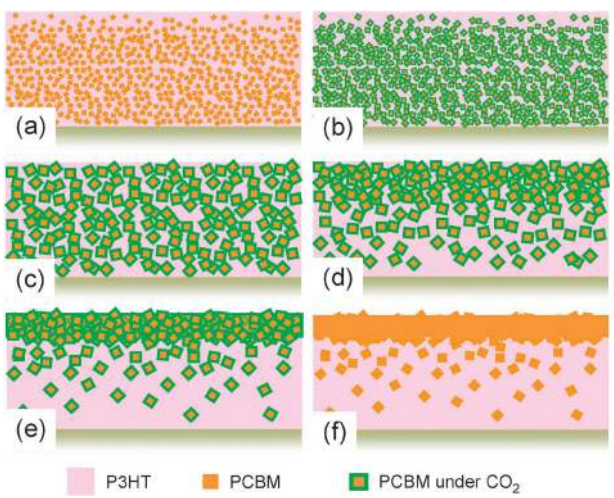

Scheme 2 Schematic representations of the steps of vertical phase separation induced by CO_2 treatment: (a) original status as cast, (b) PCBM is plasticized by CO_2 penetration, (c) plasticized PCBM aggregates in the film and P3HT domains grow larger (lateral phase separation), (d) PCBM accumulates on the surface side (vertical phase separation), (e) PCBM layer is formed, and (f) plasticized PCBM returns to normal PCBM and the stratified structure is maintained after CO_2 treatment.

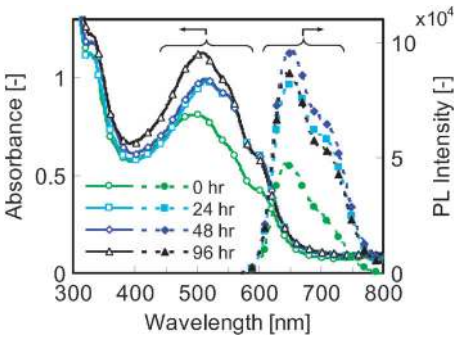

Fig. 3 Absorption and PL spectra of P3HT:PCBM films for different CO_2 treatment times.

The absorption and PL emission spectra of the film fabricated on a PEDOT:PSS/ITO/glass substrate have been shown in Fig. 3. Although these are integrated properties of the whole film thickness, spectra may reflect a PCBM layer formation. Absorption significantly increased in the range of 480 to 610 nm after 24 hour CO_2 treatment, and a further increase was observed at less than 550 nm after 96 hour treatment. The former spectrum change suggests P3HT domain growth due to PCBM aggregation, and the latter one may reflect PCBM-rich layer growth because pristine PCBM absorbs in that wavelength range once concentrated.[30] Since the spectrometer only detects transmitted light, this increased absorption spectrum technically includes an increase of reflection by the PCBM-rich layer which has a flatter surface as shown in Fig. 2d. PL emission increased (less quenching) as CO_2 treatment time increased because of phase separation while the maximum was reached by 48 hours of treatment (see ESI† for peak positions of each emission spectrum). The reason why the emission intensity of the 96 hour treated film decreased compared to the 48 hour one might be explained by the fact that the excitation light was absorbed by the PCBM-rich layer and was reflected by its surface before the light reached the underlying P3HT-rich layer. Since the film is tilted 30° with respect to the excitation light in PL measurement, the surface reflection should be more significant than those appear in absorption spectra.

Solar cells were fabricated by depositing a metal electrode on a CO_2 treated film. The device structure and approximate thickness of each layer have been shown in Fig. 4a. The performance was measured under illumination. The performance parameters including open circuit voltage (V_{OC}), short circuit current (J_{SC}), fill factor (FF), power conversion efficiency (PCE), and series resistance (R_S) are shown in Table 1, and the four current–voltage curves have been shown in Fig. 4b. While the PCE of the standard device (with as cast film) was 1.59%, a CO_2 treated device achieved up to 2.47% with a 48 hour treatment. This improvement is driven by an increase in the J_{SC}, which may come from lateral and vertical phase separation induced by CO_2 treatment. The devices with CO_2 treated films gave relatively lower V_{OC}s than the one with the as cast film did. This kind of V_{OC} drop has been also observed in other treatments such as solvent annealing,[10] where the film with proper phase separation gives relatively lower V_{OC} than the one with poor phase separation. Although this is still under considerable discussion, it has been

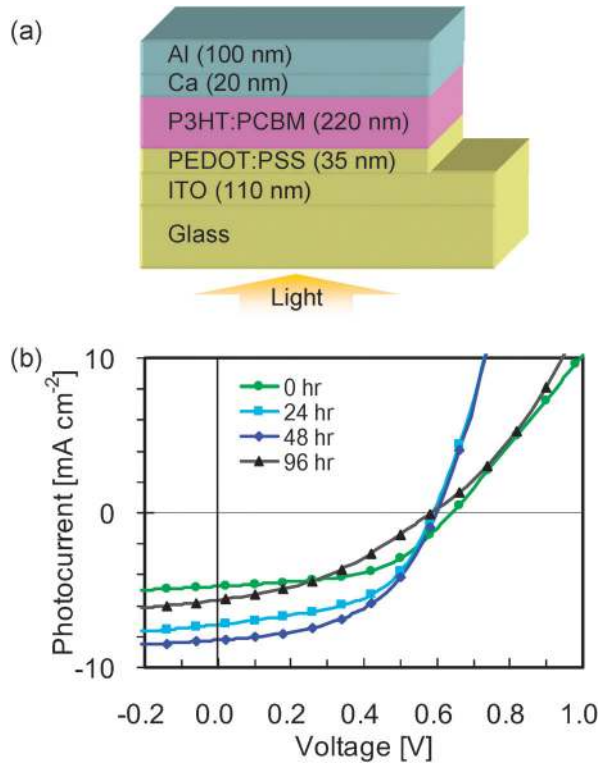

Fig. 4 (a) Device structure of the fabricated solar cells. (b) Current–voltage characteristics of P3HT:PCBM films for different CO_2 treatment times.

Table 1 Performance parameters of the solar cells with CO_2 treated films

CO_2 time/hour	V_{OC}/V	J_{SC}/mA cm^{-2}	FF [%]	PCE [%]	$R_S{}^a$/Ω cm^2
0	0.64	4.76	52.3	1.59	38.5
2	0.61	6.65	54.8	2.21	17.6
24	0.59	7.24	52.2	2.23	18.3
48	0.60	8.23	50.3	2.47	18.7
72	0.60	7.24	49.0	2.11	24.7
96	0.59	5.64	37.7	1.24	59.5

[a] Calculated as the reciprocal of the tangent line slope at V_{OC} (the point at which the current is equal to 0 mA cm^{-2}).

explained that P3HT crystallization associated with phase separation increases the interchain–interlayer (π–π) interaction which reduces the effective bandgap of the BHJ. Therefore, the performance increase in the device with the 2 hour treated film is assumed to be partly contributed by lateral phase separation. Since significant V_{OC} changes were not observed in the devices with more than 2 hour treated films, it would be presumable that lateral phase separation was saturated at the beginning of the CO_2 treatment, and further improvement in the performance is contributed by vertical phase separation. However, the PCE became worse with longer treatments, as a result of reduced J_{SC} and FF as well as increasing R_S. Longer treatments generate thicker PCBM layers on the cathode side of the film, which may increase R_S and depress FF. It may also decrease the PCBM concentration in the middle and anode side of the film and decrease the area of the donor–acceptor interface where charge separation occurs, which would result in a lower J_{SC}. As a result, 48 hours was found to be the optimum treatment time in this configuration, while the vertical profile of the obtained film may not necessarily be ideal for charge transportation.

This unique morphology induced by CO_2 treatment significantly increased the device performance, although the enhancement was not as large as the one induced by conventional treatments such as thermal annealing. Further improvement may be brought about by additional optimization of parameters such as P3HT and PCBM blend ratio, CO_2 gas pressure, and processing temperature.

Conclusions

We have demonstrated that the vertical phase separation of P3HT:PCBM blend films can be promoted by high pressure CO_2 gas at ambient temperature. Under high pressure CO_2, PCBM is selectively plasticized and its surface energy is selectively depressed, which generates a PCBM-rich layer near the surface. As the generated distribution can be preferable (not necessarily ideal) for a solar cell, it has also been shown that solar cell performance can be significantly improved by CO_2 treatment. The CO_2 treatment we present here is a very unique process to control the morphology of BHJ films because of their temperature and generated distribution. While we have applied this process to improve P3HT–PCBM based polymer solar cell performance, it also may be applicable to other polymer systems. This study demonstrates a very promising approach to address the vertical phase separation problem in BHJ polymer solar cells to enhance the efficiency.

Experimental

Substrate preparation

Samples for contact angle, XPS, optical microscope, AFM, solar cells, absorption, and PL were fabricated onto 15 mm^2 glass substrates partly covered with approximately 110 nm thick ITO. These substrates were cleaned by sonication in diluted detergent, de-ionized water, acetone, and isopropyl alcohol for 15 min each. After drying, the substrates were treated with UV-ozone for 15 min prior to spin-coating. On glass/ITO substrates, PEDOT:PSS (Baytron-P 4083) was spin-coated at 4000 rpm for 40 s, and annealed at 120 °C for 15 min. The thickness of PEDOT:PSS was approximately 35 nm. Samples for SEM and SIMS were fabricated onto a 15 mm^2 size silicon (100) substrate prepared through the same procedure as glass/ITO substrates except for PEDOT:PSS coating, and the surface should be naturally oxidized.

Sample film fabrication

The P3HT used in these experiments was obtained from Rieke Metals (4002-E, 90–94% regioregularity, average molecular weight is 5 × 10^4 g mol^{-1}). The PCBM was obtained from Nano-C. Dichlorobenzene (DCB, Sigma-Aldrich, anhydrous grade, 99% purity) was used as solvent. The solution for pristine P3HT films was prepared with 2.4 wt% P3HT in DCB (24 mg mL^{-1}), the one for pristine PCBM films was prepared with 2 wt% PCBM in DCB (20 mg mL^{-1}), and one for P3HT:PCBM blend films was prepared with 2.4 wt% P3HT and 2.4 wt% PCBM (1 : 1 ratio) in DCB. Films were fabricated in a nitrogen atmosphere. Pristine P3HT films and

P3HT:PCBM blend films were spin-coated at 900 rpm for 30 s, followed by spinning at 1500 rpm for 1 s, then they were dried by continued spinning at 600 rpm for 60 s under ambient temperature. Pristine PCBM films were spin-coated at 2000 rpm for 60 s. The typical thicknesses of P3HT:PCBM blend, pristine P3HT, and pristine PCBM were 220 nm, 180 nm, 50 nm respectively.

CO_2 treatment

Sample films were put into a Parr 4592 microreactor (approximately 78 mL inner volume) connected with a CO_2 cylinder (Air Liquid, 99.99% purity). After purging the existing gas, the vessel was filled with 4.8 MPa pressure (gas phase) CO_2, sealed and kept under ambient temperature (20 °C) for the prescribed time.

Film characterization

The film thickness was measured with a Bruker Dektak-150 profilometer. SIMS measurements were performed by Evans Analytical Group. Contact angle analysis was performed with VCA Optima XE from AST products, Inc. De-ionized water was used as liquid, and the drop volume was about 1 μL. The XPS measurements were performed with the Omicron XPS/UPS system. The pressure of the measurement chamber was maintained less than 10^{-9} mbar. A monochromatic Al Kα (1486.6 eV) X-ray source was used for excitation. The C 1s and S 2p regions were scanned with the resolution of 0.02 eV. Cross-sectional SEM samples were prepared by fracturing followed by sputtering 5 nm of Au. The images were taken using an FEI Nova Nano SEM 230 scanning electron microscope. AFM images were taken using a Bruker Dimension 5000 scanning probe microscope. Optical microscopic images were taken using a Diagnostic Spot Insight 2.0 Mp color CCD camera attached to a Nikon Eclipse E800 microscope. All absorption spectra of sample films were acquired including ITO/glass substrates and PEDOT:PSS layer using a Hitachi U-4100 spectrometer. PL spectra were acquired using a Horiba Jobin Yvon Nanolog fluorescence spectrophotometer with the sample tilted 30° with respect to the excitation beam (510 nm) and 60° with respect to the detector. All PL spectra were divided by their absorbance at 510 nm acquired from absorption spectra so that the intensity could be comparable among samples.

Solar cell characterization

The cathode electrode (20 nm thickness of Ca and 100 nm thickness of Al) was deposited on a CO_2 treated film using vacuum evaporation. The active device area of all solar cells was fixed to 0.1 cm^2. Current–voltage (*J–V*) characteristics of solar cells were measured with a Keithley 2400 source meter under the 100 mW cm^{-2} illumination generated by a Newport Oriel 91191-1000 solar simulator with an AM1.5G filter.

Acknowledgements

The authors would like to thank Dr S. Murase for technical discussion and assistance with AFM observation, K. C. Cha for taking SEM images, W. Yang for taking XPS data, L. Dou and E. Richard for valuable input, and Evans Analytical Group for performing SIMS analysis. In addition, R. Kokubu would also like to thank Furukawa Electric Co., Ltd. for granting him sabbatical leave for conducting this research.

References

1 C. J. Brabec, N. S. Sariciftci and J. C. Hummelen, *Adv. Funct. Mater.*, 2001, **11**, 15–26.
2 S. Günes, H. Neugebauer and N. S. Sariciftci, *Chem. Rev.*, 2007, **107**, 1324–1338.
3 T. Ameri, G. Dennler, C. Lungenschmied and C. J. Brabec, *Energy Environ. Sci.*, 2009, **2**, 347–363.
4 G. Yu, J. Gao, J. C. Hummelen, F. Wudl and A. J. Heeger, *Science*, 1995, **270**, 1789–1791.
5 P. Schilinsky, C. Waldauf and C. J. Brabec, *Appl. Phys. Lett.*, 2002, **81**, 3885–3887.
6 C. J. Brabec, S. Gowrisanker, J. J. M. Halls, D. Laird, S. J. Jia and S. P. Williams, *Adv. Mater.*, 2010, **22**, 3839–3856.
7 S. E. Shaheen, C. J. Brabec, N. S. Sariciftci, F. Padinger, T. Fromherz and J. C. Hummelen, *Appl. Phys. Lett.*, 2001, **78**, 841–843.
8 L.-M. Chen, Z. Xu, Z. Hong and Y. Yang, *J. Mater. Chem.*, 2010, **20**, 2575–2598.
9 G. Li, V. Shrotriya, J. Huang, Y. Yao, T. Moriarty, K. Emery and Y. Yang, *Nat. Mater.*, 2005, **4**, 864–868.
10 G. Li, Y. Yao, H. Yang, V. Shrotriya, G. Yang and Y. Yang, *Adv. Funct. Mater.*, 2007, **17**, 1636–1644.
11 F. Padinger, R. S. Rittberger and N. S. Sariciftci, *Adv. Funct. Mater.*, 2003, **13**, 85–88.
12 W. Ma, C. Yang, X. Gong, K. Lee and A. J. Heeger, *Adv. Funct. Mater.*, 2005, **15**, 1617–1622.
13 S. Miller, G. Fanchini, Y.-Y. Lin, C. Li, C.-W. Chen, W.-F. Su and M. Chhowalla, *J. Mater. Chem.*, 2008, **18**, 306–312.
14 J. Peet, J. Y. Kim, N. E. Coates, W. L. Ma, D. Moses, A. J. Heeger and G. C. Bazan, *Nat. Mater.*, 2007, **6**, 497–500.
15 Y. Yao, J. H. Hou, Z. Xu, G. Li and Y. Yang, *Adv. Funct. Mater.*, 2008, **18**, 1783–1789.
16 P. G. Karagiannidis, D. Georgiou, C. Pitsalidis, A. Laskarakis and S. Logothetidis, *Mater. Chem. Phys.*, 2011, **129**, 1207–1213.
17 H. Wang, E. D. Gomez, J. Kim, Z. Guan, C. Jaye, D. A. Fischer, A. Kahn and Y-L. Loo, *Chem. Mater.*, 2011, **23**, 2020–2023.
18 J. K. Lee, W. L. Ma, C. J. Brabec, J. Yuen, J. S. Moon, J. Y. Kim, K. Lee, G. C. Bazan and A. J. Heeger, *J. Am. Chem. Soc.*, 2008, **130**, 3619–3623.
19 M. C. Quiles, T. Ferenczi, T. Agostinelli, P. G. Etchegoin, Y. Kim, T. D. Anthopoulos, P. N. Stavrinou, D. D. C. Bradley and J. Nelson, *Nat. Mater.*, 2008, **7**, 158–164.
20 N. D. Treat, M. A. Brady, G. Smith, M. F. Toney, E. J. Kramer, G. J. Hawker and M. L. Chabinyc, *Adv. Energy Mater.*, 2011, **1**, 82–89.
21 K. H. Lee, P. E. Schwenn, A. R. G. Smith, H. Cavaye, P. E. Shaw, M. James, K. B. Krueger, I. R. Gentle, P. Meredith and P. L. Burn, *Adv. Mater.*, 2011, **23**, 766–770.
22 M. Shakutsui, T. Iwamoto, R. Maeda, T. Tsutsui and K. Fujita, *Proc. SPIE*, 2008, **7052**, 705215.
23 W.-C. V. Wang, E. J. Kramer and W. H. Sachse, *J. Polym. Sci., Polym. Phys. Ed.*, 1982, **20**, 1371–1384.
24 J. S. Chiou, J. W. Barlow and D. R. Paul, *J. Appl. Polym. Sci.*, 1985, **30**, 2633–2642.
25 A. Bos, I. G. M. Pünt, M. Wessling and H. Strathmann, *J. Membr. Sci.*, 1999, **155**, 67–78.
26 K. Mizoguchi, T. Hirose, Y. Naito and Y. Kamiya, *Polymer*, 1987, **28**, 1298–1302.
27 G. Teramoto, T. Oda, H. Saito, H. Sano and Y. Fujita, *J. Polym. Sci., Part B: Polym. Phys.*, 2004, **42**, 2738–2746.
28 D. M. DeLongchamp, R. Joseph Kline and A. Herzing, *Energy Environ. Sci.*, 2012, **5**, 5980–5993.
29 J.-N. Audinot, P. Lévêque, R. Bechara, N. Leclerc, J. Guillot, H.-N. Migeon, G. Hadziioannou and T. Heiser, *SIA Surf. Interface Anal.*, 2010, **42**, 1010–1013.
30 S. Cook, H. Ohkita, Y. Kim, J. J. B. Smith, D. D. C. Bradley and J. R. Durrant, *Chem. Phys. Lett.*, 2007, **445**, 276–280.